A Breathing Sphere Model for Calculating Frequency Shifts of Polyatomic Molecules in Solution

George S. Devendorf*

Department of Chemistry, Middle Tennessee State University, Murfreesboro, Tennessee 37132

Received: May 16, 2000; In Final Form: September 13, 2000

Molecular vibrational frequency shifts are modeled by treating the vibrating solute as a breathing sphere with repulsive (hard-core) and attractive (mean field) solvent−solute interactions. The solvent-induced repulsive force exerted on the normal mode of a vibrating solute molecule is obtained using the derivative of the molecular volume with respect to the normal mode coordinate in conjunction with an analytical expression for the chemical potential of a hard sphere solute immersed in a solvent of hard spheres. The volume derivative of the vibrating solute molecule is calculated by considering the solvent molecule as an assembly of interpenetrating or fused hard spheres whose individual motions are given by normal mode coordinates. The calculation of the repulsive force is simplified by equating the normal mode volume change of the multisphere solute to a volume change of a spherical solute. The anisotropy of the solute−solvent system is used to adjust the spherical solute diameter so its chemical potential matches the chemical potential of the multisphere solute. This adjustment is critical to correctly scale the spherical volume change to the anisotropy of the polyatomic solute. For the diatomic solutes, N_2 and HCl, the breathing sphere model predicts repulsive forces and frequency shifts that closely agree with a near exact diatomic hard sphere model. Applied to the three different CO_2 vibrations, the explicit calculation of the different excluded volume changes associated with each vibration gives predicted frequency shifts that agree with available pressure-dependent frequency data.

I. Introduction

Changes in the molecular spectra of solute molecules are an important experimental probe of intermolecular interactions in the liquid state. Gas-to-liquid vibrational frequency shifts provide a quantitative measure of the mean force exerted by a solvent on a vibrating solute and an experimental test of solvent−solute interaction models.[1] Hard sphere fluids are useful model fluids for calculating repulsive interactions between the solvent and the solute,[2,3] but analytical solutions of the solvent-induced repulsive force on the vibrating solute have been limited primarily to diatomic solute forms.[4,5] This paper describes a breathing sphere solute model that is more generally applicable to the variety of complex motions associated with normal vibrational modes of polyatomic solutes. In the breathing sphere model, the volume derivative of a vibrating polyatomic solute, $\partial V^x/\partial Q$, is used within a hard sphere model to estimate the repulsive force exerted by the solvent on the solute vibrational mode, Q, and the effect of this force on the observed gas-to-liquid vibrational frequency shift. The breathing sphere model is patterned after other hard sphere models in which attractive interactions are treated as a mean field continuum.[4,5] The strength of the attractive interactions are expressed using a single parameter whose magnitude is normally fixed using experimental frequency data.

Schweizer's and Chandler's seminal work[4] concerning solvent effects on molecular vibrations underscores the importance of repulsive solvent−solute interactions on molecular vibrations and how hard sphere fluids can be used to estimate these forces. In their work, the force along the bond of a diatomic solute represented by two overlapping spheres (or cavities) is calculated using the cavity distribution function of two interpenetrating hard spheres in a hard sphere solvent. This approach has been used in modeling solvation effects on diatomic and polyatomic solutes by Chandler and others,[4,6−12] particularly Ben-Amotz and co-workers,[13−16] who extended Chandler's original work by developing closed analytical expressions for the average hard sphere force along the "bond" separating the solute spheres.[5] Polyatomic solutes have been adapted to the two-cavity model by representing the polyatomic as a pseudodiatomic, in which each cavity represents a group of atoms in the polyatomic molecule on either side of the bond of interest.[4,14,16,17] Density-dependent frequency shifts of a number of polyatomic stretching vibrations, including ring breathing modes,[6,7] can be reproduced in this way. These successes can be attributed in part to the semiempirical nature of the model in which the effect of attractive interactions and the magnitude of the overall shift is determined empirically using at least one experimental frequency measurement. Thus, while density-dependent trends in many polyatomic frequency shifts can be reproduced, some uncertainty in the absolute magnitudes of the calculated repulsive shifts remains.[18] The pseudodiatomic adaptation relies on the assumption that the change in the polyatomic solute volume with vibrational excitation is similar to the change of a simple bond stretch of a diatomic with a volume similar to that of the polyatomic. While this may be true for some symmetric stretching modes, its validity cannot be assumed for all such vibrations, especially for nonlinear groups of bonds in which multiple overlaps of spheres representing individual atoms produce volume changes different than those produced by the single overlap of two spheres.

The breathing sphere model proposed in this work seeks to address the shortcomings of the pseudodiatomic adaptation by

10.1021/jp001802j CCC: $19.00
Published on Web 11/01/2000

incorporating the explicit volume change associated with a particular polyatomic vibration into the calculation of the repulsive force. The polyatomic volume change associated with a specific vibrational mode, Q_k, is calculated using a hard fused sphere polyatomic whose individual atomic spheres follow the motions dictated by Q_k. The polyatomic volume derivative is equated to an equivalent, "breathing sphere" derivative, $\partial V^x/\partial\sigma_o$, where the change in the spherical solute diameter, σ_o, is scaled such that $\partial V^x/\partial\sigma_o = \partial V^x/\partial Q_k$. (The relevant volume, V^x, is the volume the solute excludes from the solvent centers.) The breathing sphere model assumes that the volume change associated with a vibrational excitation is the key parameter in determining the repulsive force on that vibration and that both the volume change and related repulsive force can be adequately represented using a spherical solute. Within these constraints, the breathing sphere model yields better estimates of the mean repulsive force exerted by the solvent on different vibrational modes, more accurate repulsive frequency shifts, and improved attractive parameters that will allow better assessment of attractive interactions in future work.

The transformation from a fused-sphere to spherical solute derivative simplifies the calculation of the solvent-induced repulsive force while preserving the volume change associated with the multidimensional polyatomic vibration. The validity of a spherical representation of a multisphere solute depends in a large part to the degree and manner in which the solute anisotropy is averaged over the different solvent configurations of the fluid. If specific orientation forces are small, the anisotropy of the solute is due chiefly to its aspherical shape, and adjustments in a spherical solute diameter can compensate for the solute's asphericity.[2] Molecular simulations of fused-sphere solutes in spherical solvents show that a representative hard sphere solute with equal excluded volume has a hard sphere or excess chemical potential slightly greater than that of the fused sphere solute.[20,21] A small reduction in the solute's hard sphere diameter is therefore necessary to equate the chemical potentials of the hard sphere and fused sphere solutes. The required diameter correction has been observed to be proportional to the excluded volume anisotropy of the fused sphere solute.[21,22] While various measures of anisotropy can be employed, this study uses the difference in solute diameters based on the fused sphere solute volume and spherical excluded volume. This measure is an integral part of the breathing sphere calculation and provides a simple correction for moderately anisotropic solutes over the entire gas-to-liquid density range. As will be seen in the ensuing discussion, small adjustments ($\approx$1%) in the breathing sphere diameter yield significant differences in the calculated force and are thus an essential part of the breathing sphere calculation.

The remainder of this paper is organized as follows: Section II outlines breathing sphere repulsive force and frequency shift calculations. Diameter corrections based on the excluded volume anisotropy are discussed in section IIB. Section IIIA discusses breathing sphere results for the diatomic solutes, N_2 and HCl, and compares them to a perturbed hard fluid (PHF) model that is essentially exact for diatomic solutes.[5] In section IIIB, the breathing sphere model is applied to the three different normal modes of CO_2 and compared to available density-dependent frequency shift data. Results and conclusions are summarized in section IV.

II. The Breathing Sphere Model

IIA. Repulsive Force Calculations. Approximating repulsive forces in solution by a reference hard sphere fluid composed of spheres of an appropriate diameter is well-established.[3] The solvent-averaged repulsive force on a solute ($\langle F_{rep}\rangle$) is therefore equated to a hard sphere force defined by the derivative of the hard sphere chemical potential with respect to its diameter, σ_o.

$$\langle F_{rep}\rangle \approx F_{HS} = \left(\frac{\partial\mu_{HS}}{\partial\sigma_o}\right) \tag{1}$$

An equation for the hard sphere chemical potential of a solute at infinite dilution in a solvent of hard spheres with diameter, σ_s, and number density, ρ, can be derived from the Boublik−Mansoori−Carnahan−Starling−Leland equation of state for mixed hard spheres,[23,24]

$$\frac{\mu_{HS}}{k_BT} = \frac{2\eta d^3}{(1\text{-}\eta)^3} + \frac{3\eta d^2}{(1\text{-}\eta)^2} + \frac{3\eta d(1+d-d^2)}{(1\text{-}\eta)} + (3d^2 - 2d^3 - 1)\ln(1\text{-}\eta) \tag{2}$$

$$\frac{1}{k_BT}\left(\frac{\partial\mu_{HS}}{\partial\sigma_o}\right) = \frac{1}{\sigma_s}\left\{\frac{6\eta d^2}{(1\text{-}\eta)^3} + \frac{6\eta d^2}{(1\text{-}\eta)^2} + \frac{3\eta(1+2d-3d^2)}{(1\text{-}\eta)} + 6(d\text{-}d^2)\ln(1\text{-}\eta)\right\} \tag{3}$$

where $d = \sigma_o/\sigma_s$, $\eta = 6\pi\rho\sigma_s^3$, and k_B and T are Boltzmann's constant and the Kelvin temperature, respectively. The above expressions agree with chemical potentials obtained via computer simulations spanning gas to liquid-like densities and $d = 0.5$ to $d = 1$.[25] To model real fluids, solvent diameters derived from equation of state data provide diameters representative of molecules in the liquid state.[26,27] The best value for the solute diameter, however, depends on the solute's excluded volume anisotropy, which is discussed in section IIB.

To model the vibrating solute as a breathing sphere, the diameter change of the breathing sphere is correlated to the kth normal mode, Q_k, of the polyatomic solute.

$$F_{HS}(Q_k) = \left(\frac{\partial\mu_{HS}}{\partial Q_k}\right) = \left(\frac{\partial\mu_{HS}}{\partial\sigma_o}\right)\left(\frac{\partial\sigma_o}{\partial Q_k}\right) \tag{4}$$

Equation 4 transforms the generalized solvent force on a spherical solute into the desired solvent-induced force on the normal coordinate, Q_k. Evaluating the derivative, $\partial\sigma_o/\partial Q_k$, requires a knowledge of how the volume of the polyatomic solute (and hence the magnitude of the representative diameter, σ_o) changes with Q_k. Because the solute chemical potential depends on both solvent and solute, the volume the solute excludes from the solvent centers is the relevant volume and $\partial\sigma_o/\partial Q_k$ can be written as

$$\left(\frac{\partial\sigma_o}{\partial Q_k}\right) = \left(\frac{\partial\sigma_o}{\partial V^x}\right)\left(\frac{\partial V^x}{\partial Q_k}\right) \tag{5}$$

where "x" superscripts are used to denote quantities related to the solute excluded volume. The working equation of the breathing sphere model is obtained by substituting eq 5 into eq 4. This simple chain rule result is exact in the low density limit

$$\frac{F_{HS}(Q_k)}{k_BT} = \left(\frac{\partial\mu_{HS}}{\partial Q_k}\right) = \left(\frac{\partial\mu_{HS}}{\partial\sigma_o}\right)\left(\frac{\partial\sigma_o}{\partial V^x}\right)\left(\frac{\partial V^x}{\partial Q_k}\right) \tag{6}$$

and yields viable results at high densities for moderately aspherical solutes (see section IIIA). The density dependence is contained within the spherical derivative, $\partial\mu_{HS}/\partial\sigma_o$ (eq 3),

TABLE 1: Molecular Parameters Used in Breathing Sphere Calculations[a]

			CO_2 (neat)		
	N_2 (neat)	HCl in Ar	Q_1	Q_2	Q_3
σ_s (Å)	3.4424[26]	3.2415[26]	3.6465[27]		
σ_1 (Å)	2.99[28]	1.98[28]	3.0764[28]		
σ_2 (Å)	2.99[28]	3.4[28]	2.7145[28]		
σ_o (Å)	3.4789	3.4848	3.7474		
r_e (Å)	1.0977[15]	1.2746[34]	1.1621[41]		
ν_e (cm^{-1})	2358.57[15]	2990.95[34]	1354.91[42]	673[42]	2396.49[42]
ν_o (cm^{-1})	2329.91[15]	2886.0[34]	1332.9[41]	667.4[41]	2349.1[41]
f (10^5 d cm^{-1})	22.95[15]	5.164[34]	17.3	0.945	16.3
g (10^{13} d cm^{-2})	−56.69[15]	−9.580[34]	−37.9[33]	−1.07	−43.4
C_1	0.3978	0.2330	0.3437	0.1006	0.07364
C_2 (Å^{-2})	−0.0914	0.1140	−0.0463	0.0607	−0.00213
C_a (cm^{-1} nm^3)	0.2242	0.825	0.02	0.48	0.006

[a] Superscripts attached to table entries denote references from which data was obtained. Other entries are calculated as described in the text.

while the derivatives of eq 5 provide the necessary functional dependence on solute geometry, Q_k, and excluded volume.

Both the solute volume and the excluded volume are calculated by considering the solute as an assembly of interpenetrating or fused spheres at a particular solute geometry. Ratios of atomic diameters for the solute spheres are obtained from volume increment data,[28] and solute hard sphere volumes are obtained from tabulations of hard sphere diameters.[26,27] Absolute hard sphere values for the atomic diameters are obtained by adjusting atomic diameters (maintaining their fixed ratios from ref 28) to give a fused sphere volume consistent with the hard sphere volume of the molecule (obtained from molecular diameters of ref 26 or 27). The excluded volume is obtained using excluded volume diameters for each solute atom, σ_i^x, which are the sum of the solute atom diameter and solvent diameter, $\sigma_i^x = \sigma_i + \sigma_s$. Details of volume calculations are contained in the appendix and relevant diameters are given in Table 1.

IIB. Anisotropy Corrections to the Solute Diameter. For a spherical solute, the excluded volume diameter, $\sigma^x = (6V^x/\pi)^{1/3}$, is the sum of the solute diameter, $\sigma_q = (6V_q/\pi)^{1/3}$, and solvent diameter, σ_s: $\sigma^x = \sigma_s + \sigma_q$, where the subscript, q, refers to a specific atomic geometry of the solute and labels fused sphere solute quantities. In the spherical solute case, $\sigma_q = \sigma_o$, and because σ_s is constant,

$$\left(\frac{\partial\sigma_o}{\partial V^x}\right) = \left(\frac{\partial\sigma_q}{\partial V^x}\right) = \left(\frac{2}{9\pi}(V^x)^{-2}\right)^{1/3} \tag{7}$$

For a nonspherical solute composed of several fused spheres, however, $\sigma^x > \sigma_s + \sigma_q$, and a new solute diameter, $\sigma_q^x = \sigma^x - \sigma_s$, must be defined which is consistent with the larger excluded volume of the fused sphere solute. The diameter, σ_q^x, corresponds to a spherical solute with an excluded volume equal to the excluded volume of the fused sphere solute. This diameter must be decreased slightly for the spherical chemical potential to match that of the fused sphere solute.[20,21] Ben-Amotz and Stamatopoulou[21,22] used a scaled surface area measurement of the anisotropy to adjust σ_q^x, but the difference between the two solute diameters, $\delta_q = \sigma_q^x - \sigma_q$, provides a very similar measure of the excluded volume anisotropy. Using δ_q, a satisfactory formula for the anisotropy corrected solute diameter is given by

$$\sigma_o = \sigma_q^x - \frac{\delta_q}{(\sigma_s + 1)} \tag{8}$$

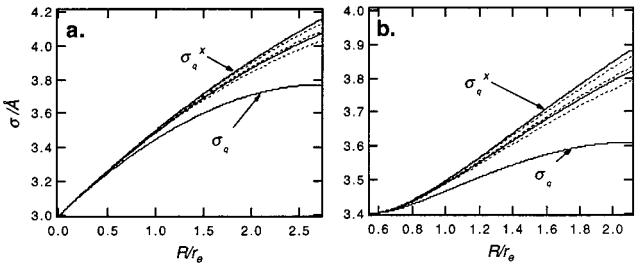

Figure 1. Plots of solute diameters for hard sphere systems representing neat N_2 (a) and HCl in Ar (b) as a function of the reduced bond length. Lower curves are spherical solute diameters based on the fused sphere solute volume, and upper curves are solute diameters based on excluded volumes of the fused sphere solute. The middle curves represent anisotropy corrected diameters. The solid curve is given by eq 8, and dotted curves are density-dependent diameters from ref 21. Note that the range of the diameter scale for N_2 is twice that of HCl's.

Equation 8 is purely empirical but provides a simple prescription for obtaining σ_o. The factor of 1 in the denominator is required to make the anisotropy correction go to zero in the limit of small σ_s and also gives the most satisfactory results of several anisotropy corrections investigated. The central derivative of eq 6 is now

$$\left(\frac{\partial\sigma_o}{\partial V^x}\right) = \left(\frac{2}{9\pi}(V^x)^{-2}\right)^{1/3} - \frac{1}{(\sigma_s + 1)}\left(\frac{\partial\delta_q}{\partial V^x}\right) \tag{9}$$

and contains an anisotropy term that is numerically evaluated in this study.

Figure 1 shows calculated solute diameters for hard sphere systems representing neat N_2 and HCl in argon as a function of the reduced bond length, R/r_e, of the fused sphere diatomic. (r_e is the equilibrium bond length of the gas phase molecule.) The bond length coordinate goes from fully enmeshed atoms (a spherical solute) to contact separation and thus also represents a scale of increasing solute anisotropy. The upper and lower solid curves in each plot represent the solute diameters, σ_q^x and σ_q, respectively, while the middle solid curve represents σ_o given by eq 8. The dotted curves represent diameters corrected according to the prescription given by ref 21, where the anisotropy correction was scaled so that the chemical potential of the spherical solute exactly matches the chemical potential of a fused sphere diatomic with volume, V_q, and excluded volume, V^x. A mild density dependence is required in the corrected solute diameters for the spherical chemical potentials to exactly match hard diatomic chemical potentials at all densities. The dotted curves therefore represent corrected diameters at the reduced densities, $\rho^* = 0.3$, 0.6, and 0.9, where larger corrections (lower curves) correspond to higher densities ($\rho^* = \rho\sigma_s^3$). The density-independent diameter of eq 8 corresponds to a density-dependent correction at $\rho^* \approx 0.68$, which is very close to normal liquid densities and, at the equilibrium bond lengths, provides an average diameter correction sufficient to predict density-dependent shifts up to $\rho^* \approx 1.0$ (see section IIIA). Because the differences in all diameters diverge as the anisotropy increases, a density-dependent correction should be considered for reduced densities greater than 1.0 or for highly anisotropic solutes.

IIC. Frequency Shift Calculations. Frequency shift calculations closely follow methods outlined in the perturbed hard fluid (PHF) model.[5] Using second-order perturbation theory, Buckingham[29] derived an expression for the frequency shift of a cubic

diatomic oscillator due to a perturbing solvent potential, U,

$$\frac{\Delta\nu}{\nu_e} = \frac{3}{2}\frac{g}{f^2}F + \frac{1}{f}G \tag{10a}$$

where f and g are the quadratic and cubic force constants of the gas-phase vibrational potential, and ν_e is the harmonic gas-phase frequency. F and G are given by the solvent-averaged derivatives of U,

$$F = \left\langle \left(\frac{\partial U}{\partial R}\right)_{r_e} \right\rangle, \; G = \frac{1}{2}\left\langle \left(\frac{\partial^2 U}{\partial R^2}\right)_{r_e} \right\rangle \tag{10b}$$

where R is the bond length of the diatomic solute, and the derivatives are evaluated at the equilibrium bond length, r_e. The first derivative of U is the force the surrounding solute exerts along the diatomic bond and, in the first term of eq 10, contributes 70% or more to the total frequency shift.[16] The quantity, $1/2(\partial F/\partial R)_{r_e}$, is a mean field approximation for G used in this work and is negative for homonuclear diatomics but can be positive or negative for other molecules (see Figures 3 and 5). While this approximation probably underestimates the magnitude of G, which should also include a positive fluctuation term,[30] the contribution of G to the overall shift is small, and such an omission has negligible effects on most predicted frequency shifts.

The calculated frequency shift is broken into repulsive and attractive parts corresponding to the repulsive and attractive parts of the solvent−solute interaction. The repulsive part of the frequency shift is calculated by setting F of eq 10b equal to $F_{HS}(Q)$ of eq 6. (The single vibrational mode of the diatomic is labeled by the bond length, R.) Using the density independent σ_o given by eq 8, the density-dependent repulsive F and G terms of eq 10b can be expressed as

$$F_{rep} = k_B T\left(\frac{\partial \mu_{HS}}{\partial \sigma_o}\right)C_1 \tag{11a}$$

$$G_{rep} = \frac{k_B T}{2}\left\{\left(\frac{\partial^2 \mu_{HS}}{\partial \sigma_o^2}\right)C_1^2 + \left(\frac{\partial \mu_{HS}}{\partial \sigma_o}\right)C_2\right\} \tag{11b}$$

where C_1 and C_2 are density-independent constants determined at the equilibrium nuclear configuration (q_e) of the solute.

$$C_1 = \left[\left(\frac{\partial \sigma_o}{\partial V^x}\right)\left(\frac{\partial V^x}{\partial Q_k}\right)\right]_{q_e} \tag{12a}$$

$$C_2 = \left[\left(\frac{\partial^2 \sigma_o}{\partial V^{x2}}\right)\left(\frac{\partial V^x}{\partial Q_k}\right)^2 + \left(\frac{\partial^2 V^x}{\partial Q_k^2}\right)\left(\frac{\partial \sigma_o}{\partial V^x}\right)\right]_{q_e} \tag{12b}$$

The constants, C_1 and C_2, are sensitive scaling factors that adjust the spherical derivatives to match the excluded volume derivative of the fused sphere solute vibrating with the normal mode motion, Q_k.

Single force constants characterizing the normal modes of CO_2 were evaluated to utilize the diatomic form of eq 10. Results using polyatomic forms of eq 10[29,31] will be investigated in the future, but the diatomic form was retained in the transition from diatomic to polyatomic molecules in this work. Quadratic constants for each mode were calculated using $f_k = (2\pi c\nu_k)^2\mu_k$, where ν_k is the harmonic frequency of a given mode k, and the mass terms are $\mu_1 = m_O$ and $\mu_k = m_O m_C/(2m_O + m_C)$ for $k = 2$ and $k = 3$.[32] A value for the cubic constant of the ν_1 symmetric stretch was obtained from ref 33, and the cubic constants for other modes were calculated assuming all modes follow the relation: $g/f = A(\nu_e - \nu_o/\nu_e)$, where A is a constant determined using f_1 and g_1, and ν_e and ν_o are the harmonic and the $1 \leftarrow 0$ gas-phase transition frequencies for a given mode. Values for the vibrational constants are given in Table 1.

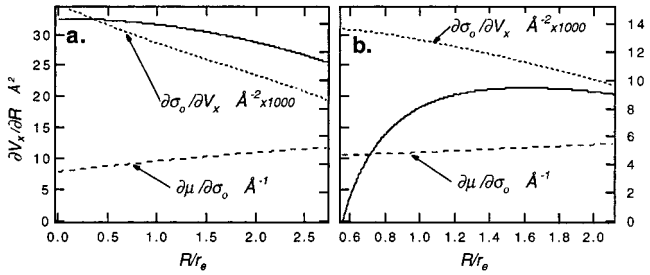

Figure 2. Derivative quantities from eq 6 plotted vs reduced bond length for N_2 (a) and HCl in Ar (b) hard sphere systems. The bond length scale extends from fully enmeshed solute atoms to atoms at contact. Solid curves are the derivatives, $\partial V^x/\partial R$, and the right-hand scale pertains to the labeled dashed curves.

The attractive portion of the frequency shift is due to a combination of dispersive, dipolar, and multipolar interactions, whose effect on the frequency shift is characterized by a single empirical parameter, C_a. If the relatively long-range attractive interactions are modeled as a mean field continuum, the attractive frequency shift is a linear function of the solvent density,[4,5]

$$\Delta\nu_a = C_a\rho \tag{13}$$

and both $\Delta\nu_a$ and C_a are determined using experimental frequency data and calculated repulsive shifts. For simple systems such as neat N_2, empirical C_a values have been reproduced using a simple dispersion formula.[15] Generally C_a values are more difficult to predict[13,19] and the improved repulsive shifts of the breathing sphere model will enable a more accurate partitioning of polyatomic frequency shifts into repulsive and attractive parts and better empirical assessments of C_a for different polyatomic vibrations.

III. Results and Discussion

IIIA. Diatomic Solutes. Breathing sphere calculations were done on systems representing neat N_2 and HCl in Ar to examine the functionality of the breathing sphere model on the vibrational coordinate, R, and to compare breathing sphere calculations to PHF results and experimental frequency shifts. Figure 2 shows the three derivative quantities of eq 6 plotted against the reduced separation of the solute atoms at a reduced solvent density of 0.7. The functional behavior of the repulsive force (shown in Figure 3) is shaped primarily by the volume derivative, $\partial V^x/\partial R$ (solid curves in Figure 2), which passes through a maximum when the diameter of the smaller solute atom intersects the surface of the larger atom. For a homonuclear diatomic, this occurs at $R = 0$, while increasing differences in size between the solute atoms shifts the maximum in $\partial V^x/\partial R$ to larger values of R. This functional behavior influences both the sign and magnitude of the second derivative quantity, $\partial^2\mu/\partial R$, which is twice the mean field approximation for G (eq 10b).

The solid curves in Figure 3 show $\partial\mu/\partial R$ as a function of the reduced bond length for both the N_2 and HCl/Ar hard sphere systems ($\rho^* \approx 0.7$). The breathing sphere calculations are in close agreement with PHF results (dashed curves), differing by less than 1.5% over the entire range of R examined. The dotted curves show results obtained using the uncorrected solute

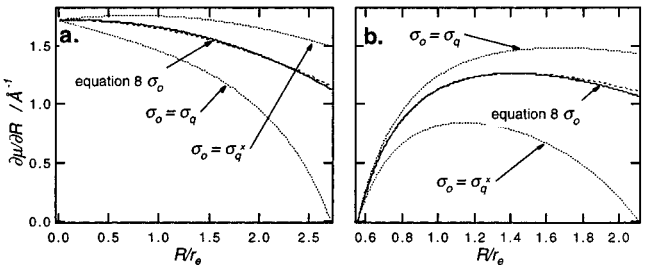

Figure 3. The repulsive hard sphere force (divided by k_BT) plotted vs reduced bond length for hard sphere systems representing neat N_2 (a) and HCl in Ar (b). The dotted curves represent calculations using uncorrected diameters, the solid curves use asymmetry corrected diameters, and the dashed curves are PHF predictions. Reduced solvent density is 0.7.

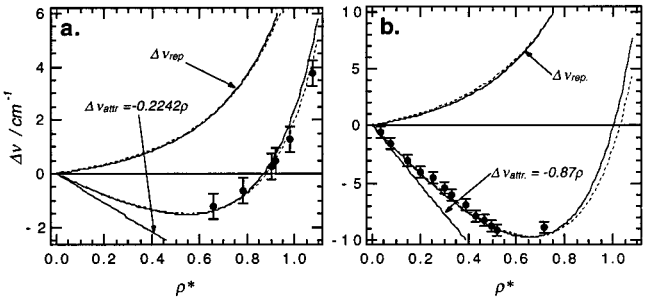

Figure 4. Calculated and experimental 295 K frequency shifts for neat N_2 (a) and HCl in Ar (b) vs reduced density. Solid curves are breathing sphere predictions, and dashed curves are PHF predictions. Both models use the same attractive force parameters.

diameters, σ_q (lower curves) or σ_q^x (upper curves). For all curves, $\partial V^x/\partial R$ is the same, and the dramatic differences in the calculated force are due to the sensitivity of the calculation to the diameter derivative, $\partial\sigma_o/\partial V^x$, rather than to the small changes ($\approx$ 1% or less at r_e) in absolute values of the different solute diameters. The scaling factors, C_1 and C_2, are thus very sensitive to the functional form of σ_o, and it is imperative that σ_o be correctly scaled to reflect both the correct solute size and the excluded volume anisotropy.

Figure 4 shows experimental and calculated density-dependent frequency shifts for N_2[15] and HCl.[34] The N_2 experimental frequency shifts range from normal liquid densities ($P \approx 1$ kbar @ 23 °C) to densities typical of highly compressed liquids ($P \approx 30$ kbar), while the HCl shifts span the density range between normal gas and liquid densities. (Ar pressures $\approx 0.01-1$ kbar.) The upper curves in the plots are the repulsive part of the frequency shift ($\Delta\nu_r$) calculated using eq 10 via the PHF (dashed curves) or breathing sphere (solid curves) model. For N_2, the attractive shift parameter was calculated using a simple dispersion formula,[15] and the predicted N_2 frequency shift calculation contains no adjustable parameters. For HCl, the attractive parameter was determined by a best fit to the experimental shifts but is less than 10% larger than an attractive parameter determined from an accurate HCl−Ar potential.[35] For both diatomics, the breathing sphere model gives results in close agreement with the PHF model, although at densities of highly compressed fluids, the breathing sphere calculations result in a slightly larger repulsive force and hence larger blue shifts. This is not surprising given that a density-independent diameter was used in the breathing sphere calculations. Using the density-dependent diameter of ref 21 gives breathing sphere results in closer agreement with PHF predictions at the high densities of compressed liquids.

IIIB. Carbon Dioxide. To apply the breathing sphere model to the different modes of vibration in a polyatomic molecule, a direct excluded volume calculation, such as performed with diatomics, is not sufficient. For example, both $\partial V^x/\partial Q_2$ and $\partial V^x/\partial Q_3$ are zero at the equilibrium geometry of CO_2 and even have negative values elsewhere. For any molecule, however, excitation to a higher vibrational state implies that the individual atoms of the molecule are sweeping out larger vibrational amplitudes. Because this occurs over time scales much faster than solvent reorientation, the net effect of the complete vibration cycle will be an increase in the excluded volume. To calculate the repulsive force, therefore, an effective $\partial V^x/\partial Q_k$ is defined in which only positive changes to the excluded volume over the complete vibrational cycle are considered. To accomplish this, the center of mass of the solute is fixed (this fixes the location of the excluded volume in the equilibrated solvent), and a Cartesian coordinate description of each atom's normal mode motion is considered rather than the simpler internal coordinate description of Q_k.

For the ν_1 mode of CO_2, the C atom remains stationary at the center of mass and a Cartesian coordinate description is equivalent to an internal coordinate description. The normal coordinate, Q_1, consists of two bond stretches, and thus $Q_1 = 2R_{CO}$ where R_{CO} is the C−O separation. The excluded volume derivative is therefore, $\partial V^x/\partial Q_1 = 0.5(\partial V^x/\partial R_{CO})$. ($Q_k$ is the sum of all atom displacements without mass weighting.) The C atom does not remain fixed in the antisymmetric stretch, ν_3, but must move in an opposite direction to the O atoms for the center of mass to remain fixed. Because the C atom is lighter than the O atoms, its relative displacement is more than twice that of a single O atom and much of the Q_3 motion consists of the oscillatory motion of the C atom, which contributes very little to changes in the excluded volume. The calculation of $\partial V^x/\partial Q_3$ is simplified by assuming the contribution of the C atom motion to $\partial V^x/\partial Q_3$ is zero, and only the small outward displacements of the O atoms need be considered. With the C atom fixed, the Q_3 calculation is similar to the symmetric Q_1 calculation, but the displacement coordinate, R_{CO}, only represents that part of the Q_3 motion contributing to a change in the excluded volume. The complete Q_3 motion (including the C atom displacement) is

$$Q_3 = 2(2x_O + x_C) = 2\left(2R_{CO} + 2\frac{m_O}{m_C}R_{CO}\right) = 9.33R_{CO}$$

where m_i and x_i are the mass and displacement of atom i, $x_O = R_{CO}$ and $\partial V^x/\partial Q_3 = 0.107(\partial V^x/\partial R_{CO})$. The first factor of 2 is required because the total positive volume change requires two vibrational displacements or one complete vibrational cycle.

The Cartesian displacements and volume calculations of the ν_2 bending mode are somewhat different than an internal bond bending description of ν_2. Just as with the ν_3 mode, the larger C atom displacement must compensate for two O atom displacements to keep the center of mass constant, but the center of mass displacements are perpendicular to the bond axis. When considering the complete vibration, the C atom displacement almost completely overlaps with the O atom displacements that are primarily directed inward. The net positive $\partial V^x/\partial Q_2$ is therefore approximated by the oscillatory motion of the C atom only, and the Q_2 calculations are based on a four-sphere volume calculation in which two spheres perpendicular to the bond axis are used to represent the C atom at each turning point of the vibration. (See Figure 8 of the appendix.)

The calculated repulsive force on the three different vibrational modes of CO_2 is shown in Figure 5. In plot a, the repulsive force for each vibrational mode is plotted versus its respective

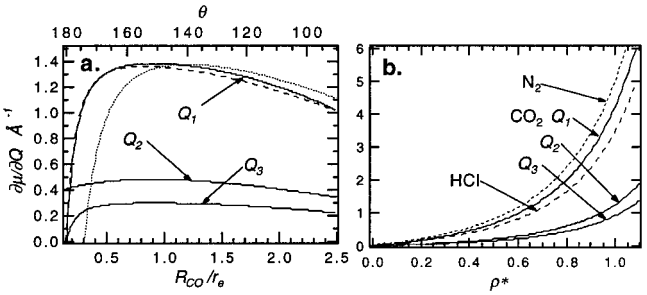

Figure 5. Calculated repulsive force (divided by k_BT) for normal modes of CO_2. Plot a shows force vs molecular coordinates at $\rho^* = 0.7$ (COC angle, θ, pertains to Q_2). Solid curves are breathing sphere calculations. Dotted and dashed curves are PHF calculations using two different pseudodiatomic forms (see text). Plot b shows density dependent force vs solvent density at equilibrium geometry of CO_2. Diatomic force curves are included for comparison.

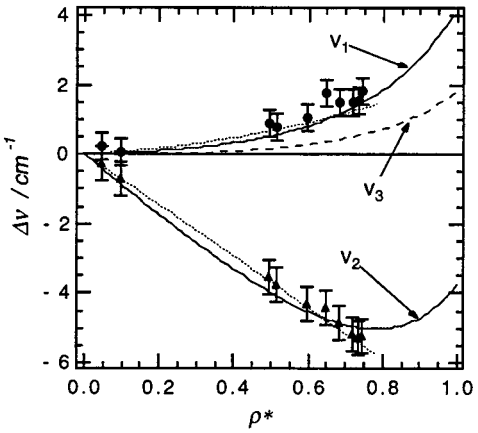

Figure 6. Density-dependent 295 K frequency shifts for ν_1, ν_2, and ν_3 modes of CO_2. Points are author's data corrected for Fermi resonance. Dotted curves are fits to average shifts taken from ref 36 (with same Fermi resonance correction applied), and solid curves are breathing sphere predictions. Dashed curve is predicted ν_3 shift.

molecular coordinate, R_{CO} or θ. Two different PHF predictions for the Q_1 symmetric stretch are also plotted: The dashed curve represents a PHF calculation for a hard sphere C−O diatomic, and the dotted curve represents the pseudodiatomic, [OC]−O. At the equilibrium bond length, the PHF calculations differ from one another by less than 0.5% (The breathing sphere calculation is $\approx$ 2% larger), but the larger [OC] sphere of the pseudodiatomic gives significant differences elsewhere along the vibrational coordinate as well as different second derivative values at r_e. The insensitivity of the PHF repulsive force calculation at r_e to variations in solute atom diameters and separations is commonly observed,[16] and the Q_1 curves in Figure 5a suggest that the importance of the model solute lies in its ability to reproduce the changing excluded volume associated with a specific solute vibration, rather than reproducing an exact solute form or volume.

The use of the C−O diatomic to model the CO_2 symmetric stretch is based on a polyatomic treatment suggested by Schweizer and Chandler,[4] in which a weighted average of separate diatomic motions is used to approximate the normal mode motion. (Two equivalent C−O stretches average to a single C−O stretch for Q_1.) The C−O diatomic and breathing sphere results are approximately the same because the overlap between the two O atoms is contained entirely within the C atom, and breathing sphere volume changes are due only to changes in two equivalent C−O overlaps. In the nonlinear Q_2 and asymmetric Q_3 motions, the breathing sphere calculation incorporates volume change differences due to nonlinear and asymmetric vibrational motions that a simple pseudodiatomic form cannot reproduce. The different form and magnitude of the Q dependent force on these vibrations is evident in Figure 5a, while Figure 5b shows the density-dependent force of each mode along with the diatomic systems discussed previously. Clearly, the smaller volume changes associated with Q_2 and Q_3 result in smaller repulsive forces, while the exact forms of the volume changes associated with each mode are important in determining second derivative terms (mean field G) for frequency shift calculations.

Experimental and predicted density-dependent frequency shifts for all three vibrational modes of CO_2 are shown in Figure 6. Predicted shifts using the breathing sphere model are shown as solid curves and points denote the authors experimental data.[36] The experimental ν_1 shifts are corrected for Fermi resonance according to a density-dependent Fermi resonance parameter given by Garrabos[37,38] and an exact Fermi resonance at a density intermediate between that of the gas and liquid. The ν_2 shifts in the figure are one-half of the Fermi resonance corrected shifts corresponding to the $2\nu_2$ overtone. The dotted curves are from polynomial fits of data (corrected for Fermi resonance) given by Garrabos[38] and span approximately the same density range as our own data. The solid and dashed curves are breathing sphere predictions. Values for C_a parameters were fixed by fitting to the experimental points and are listed in Table 1. The dashed curve represents $\Delta\nu_3$ shifts based on a C_a that gives initial red shifts ≈ -0.006 cm^{-1}/nm^{-3}, which is one-third of the average pressure-induced shift observed for individual rotational lines in the $3 \leftarrow 0$ vibrational transition in the low-pressure gas.[39] Qualitatively, the breathing sphere model appears to give shifts for all three modes consistent with existing data, although the lack of high-pressure IR frequency data makes it impossible to make quantitative judgments. Also, the density dependence of the unperturbed ν_1 and $2\nu_2$ modes is very sensitive to the Fermi resonance correction,[38] and this introduces an additional degree of uncertainty to the Fermi-corrected experimental shifts and C_a values for these modes.

Empirical C_a values are difficult to correlate to electro-optical parameters for the different vibrational modes and the expected contributions of dispersive, dipolar and multipolar interactions. Only Q_1 has a nonzero polarizability derivative at the equilibrium geometry of the molecule, yet its small C_a value suggests that dispersive interactions have a small effect on ν_1 frequency shifts. (Given the magnitude of the polarizability of CO_2, one would expect C_a values for the ν_1 mode at least as large as that for N_2.) Ab initio calculations[40] of dipole moment derivatives show the Q_2 derivative to be slightly larger than that for Q_3, but the small C_a value of ν_3 indicates that simple dipolar interactions likewise have very small effects on the ν_3 frequency shifts. Only in calculated second derivative values of the polarizability and dipole and quadrupole moments does the Q_2 mode have significantly larger values that might account for its large red shifts.

IV. Summary

The empirical C_a values and electro-optical parameters associated with each vibrational mode of CO_2 clearly demonstrates the complexity of accurately assessing the effects of repulsive and attractive solvent−solute interactions on the frequencies of polyatomic vibrational transitions. The breathing sphere model provides a simple method for estimating the repulsive part of this interaction on polyatomic vibrations. It evaluates the average solvent-induced repulsive force on a given vibration by equating the excluded volume change of a vibrating

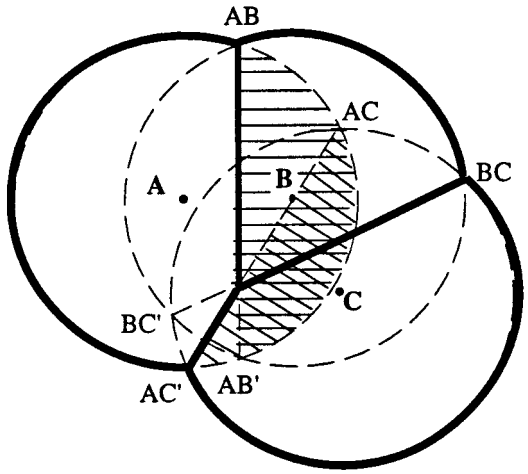

Figure 7. Cross section through centers of three overlapping spheres, A, B, and C. The triple overlap region, V_{abc}, is indicated by crosshatch marks and represents the intersection of V_{ab} (horizontal hatch marks) and V_{ac} (diagonal hatch marks). Labels refer to sphere centers and intersection points of spheres.

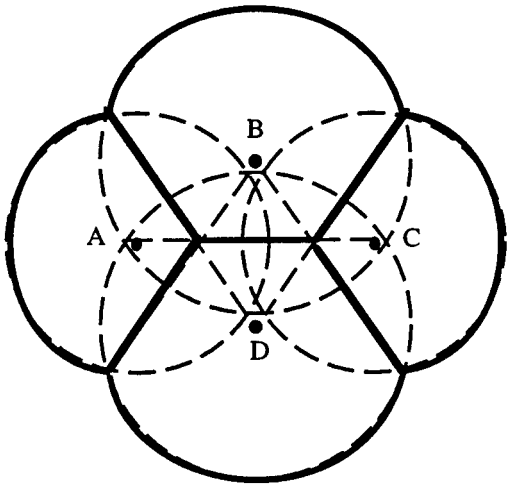

Figure 8. Four-sphere system used to calculate CO_2 Q_2 volume derivative. Heavy solid lines outline sphere segments. Volume formulas for segments are given in the text.

multisphere solute in a solvent of hard spheres to that of a breathing sphere solute, for which a relatively simple analytical solution for the solvent-induced repulsive force exists. This calculation is very sensitive to the solute diameter, whose value must be adjusted according to the anisotropy of the excluded volume of the multisphere solute. The breathing sphere model provides a simple prescription for the anisotropy adjusted solute diameter and gives results for diatomic solutes in agreement with simulation tested diatomic models over a large range of bond lengths and densities.

For CO_2, the lack of high-pressure frequency data, a density-dependent Fermi resonance interaction and possible higher order attractive effects dependent on second derivative values of electro-optical parameters complicate the comparison of breathing sphere results to existing frequency shift data. The breathing sphere treatment of CO_2 does demonstrate the model's adaptability and sensitivity to different vibrational modes and molecular geometries—features that are not present in previous diatomic adaptations to polyatomic solutes. Work continues on refining a general breathing sphere application to nonplanar polyatomics and testing the breathing sphere model against available high-pressure frequency data for polyatomic vibrations.

Acknowledgment. The author thanks Dor Ben-Amotz for helpful discussions and the MTSU research foundation for support of this work through a summer research grant.

Appendix: Fused Sphere Volume Calculations

A fused sphere volume is obtained by summing individual sphere segment volumes, V_i^{seg}. Sphere segments, whose boundaries are depicted in Figure 7 with bold lines, are obtained by removing those portions of the sphere that penetrate into neighboring sphere segments. In cases where no more than three spheres overlap as shown in Figure 7, a general formula for the volume of the ith segment is given by

$$V_i^{seg} = V_i - \sum_{j\neq 1}\left[V_{ij} - \frac{1}{2}\sum_{k\neq i,j} V_{ijk}\right] \qquad \text{(A1)}$$

where V_{ij} (horizontal and diagonal ruled regions in Figure 7) is the volume of sphere i penetrating into sphere segment j, and V_{ijk} (crosshatched area in Figure 7) is the intersection of volumes V_{ij} and V_{ik} . The factor of 1/2 in the sum over k is included because V_{ijk} and V_{ikj} represent the same volume. Additional terms must be added to eq A1 if it is to generally hold for configurations containing 4-fold and higher overlaps. Appropriate segment volumes can be obtained for any planar system using only double and triple overlap terms, however, if the sums in eq A1 are adjusted to fit a particular system of spheres. For example, triple and higher order overlaps formed by double overlaps completely contained within other double overlaps in linear and near linear systems of spheres may be ignored if only double overlaps between nearest neighbors are included in the sum over j. For nonlinear systems, however, triple overlaps are often formed from the partial overlap of two doubly overlapped regions as shown in Figure 7, and triple overlap volumes must be included in the volume calculation. For the particular case in Figure 7, the volume segments are $V_a^{seg} = V_a - V_{ab} - (V_{ac} - V_{abc})$, $V_b^{seg} = V_b - V_{ba} - (V_{bc} - V_{bca})$, and $V_c^{seg} = V_c - V_{cb} - (V_{ca} - V_{cba})$. These equations can be obtained by either visual inspection of Figure 7 or the application of eq A1where the equivalent volumes, V_{ijk} and V_{ikj}, have been combined into single terms. An example of a four-sphere system containing a 4-fold overlap is depicted in Figure 8. This configuration was used to calculate Q_2 derivative quantities for CO_2 and is a symmetrical arrangement where spheres A and C and spheres B and D are the same size. Sphere segment formulas containing only triple overlap terms were obtained by visual inspection.

$$V_a^{seg} = V_c^{seg} = V_a - V_{ab} - (V_{ad} - V_{abd})$$

$$V_b^{seg} = V_d^{seg} = V_b - V_{bd} - 2(V_{ba} - V_{bda})$$

The overlap volume, V_{ij}, for two spheres with radii, r_i and r_j, separated by the distance, r_{ij}, is

$$V_{ij} = \pi\left[\frac{2}{3}r_i^3 + l_{ij}\left(\frac{l_{ij}^2}{3} - r_i^2\right)\right], \left(l_{ij} = \frac{r_{ij}^2 + r_i^2 - r_j^2}{2r_{ij}}\right) \qquad \text{(A2)}$$

The length, l_{ij}, is the perpendicular distance from the center of sphere i to the intersection plane (or chord in Figure 7) formed by the intersection of sphere i and sphere j. Placing sphere i at the origin and defining the positive x direction to be toward the

center of sphere j, V_{ijk} is given by

$$V_{ijk} = \int_{x_{ij}}^{x_{ik}} A(x)dx + \int_{x_{ik}}^{r_i} \pi r_x^2 dx$$

$$A(x) = r_x^2\left(\frac{\pi}{2} - sin^{-1}\left[\frac{y_x}{r_x}\right]\right) - y_x(r_x^2 - y_x^2)^{1/2} \qquad \text{(A3)}$$

where $A(x)$ is the area of a slice of V_{ijk} at a given x, and the limits in the integrals correspond to the labeled intersection points in Figure 7. The Cartesian coordinates of the ij intersection points are $x_{ij} = l_{ij}$ and $y_{ij} = \pm (r_i^2 - l_{ij}^2)^{1/2}$. The ik Cartesian coordinates are obtained similarly but must be rotated through the angle jik defined by the sphere centers. The radius of the $A(x)$ slice is $r_x = (r_i^2 - x^2)^{1/2}$, and $y_x = m_{ik}x + b_{ik}$ defines a straight-line boundary of $A(x)$ where the slice intersects the plane containing chord IK. The parameters, m_{ik} and b_{ik}, are the slope and intercept, respectively, of the chord IK. The first integral in eq A3 is evaluated numerically. The second integral is required if the triple overlap region, V_{ijk}, extends over both sides of the $y = 0$ line through the centers of spheres i and j and evaluates to eq A2 with x_{ik} substituted for l_{ik}. The above treatment is applicable to any planar array of spheres of varying size and geometric arrangement.

References and Notes

(1) Maitland, G. C.; Rigby, M.; Smith, E. B.; Wakeman, W. A. *Intermolecular Forces*; Oxford University Press: New York, 1981; chapter 7.

(2) Anderson, H. C.; Chandler, D.; Weeks, J. D. *Adv. Chem. Phys.* **1976**, *34*, 105.

(3) Barker, J. A.; Henderson, D. *Rev. Mod. Phys.* **1976**, *48*, 587.

(4) Schweizer, K. S.; Chandler, D. *J. Chem. Phys.* **1982**, *76*, 2296.

(5) Ben Amotz, D.; Herschbach, D. R. *J. Phys. Chem.* **1993**, *97*, 2295.

(6) Zakin, M. R.; Herschbach, D. R. *J. Chem. Phys.* **1985**, *83*, 6540.

(7) Zakin, M. R.; Herschbach, D. R. *J. Chem. Phys.* **1986**, *85*, 2376.

(8) Zerda, T. W.; Bradey, T. M.; Jones, J. *J. Chem. Phys.* **1987**, *86*, 3219.

(9) LeSar, R. *J. Chem. Phys.* **1987**, *86*, 4138.

(10) Zakin, M. R.; Herschbach, D. R. *J. Chem. Phys.* **1988**, *89*, 2380.

(11) Ben-Amotz, D.; Zakin, M. R.; King, H. E., Jr.; Herschbach, D. R. *J. Phys. Chem.* **1988**, *92*, 1392.

(12) Meyers, A. B.; Markel, F. *Chem. Phys.* **1990**, *149*, 21.

(13) Ben-Amotz, D.; Lee, M. R.; Cho, S. Y.; List, D. J. *J. Chem. Phys.* **1992**, *96*, 8781.

(14) Lee, M. R.; Ben-Amotz, D. *J. Chem. Phys.* **1993**, *99*, 10074.

(15) Devendorf, G. S.; Ben-Amotz, D. *J. Phys. Chem.* **1993**, *97*, 2307.

(16) Hutchinson, E. J.; Ben-Amotz, D. *J. Phys. Chem. B* **1998**, *102*, 3354.

(17) Pratt, L. R.; Hsu, C. S.; Chandler, D. *J. Chem. Phys.* **1978**, *68*, 4202.

(18) Questions of the validity of the pseudodiatomic model arise from its ability to model vibrations other than simple symmetric stretches, most notably symmetric and asymmetric stretches with the same pseudodiatomic form (ref 19), its insensitivity to the exact diatomic form used (refs 13, 14, and 16) and anomolous methyl stretch behavior (ref 14).

(19) Devendorf, G. S., Ph.D. Thesis, Purdue University, 1996.

(20) Gibbons, R. M. *Mol. Phys.* **1969**, *17*, 81.

(21) Stamatopoulou, A.; Ben-Amotz, D. *J. Chem. Phys.* **1997**, *106*, 1181.

(22) Ben-Amotz, D. *J. Chem. Phys.* **1997**, *106*, 5631.

(23) Boublik, T. *J. Chem. Phys.* **1970**, *53*, 471.

(24) Mansoori, G. A.; Carnahan, N. F.; Starling, K. E.; Leland, T. W. *J. Chem. Phys.* **1971**, *54*, 1523.

(25) de Souza, L. E. S.; Stamatopoulou, A.; Ben-Amotz, D. *J. Chem. Phys.* **1994**, *100*, 1456.

(26) Ben-Amotz, D.; Herschbach, D. R. *J. Chem. Phys.* **1990**, *94*, 1038.

(27) Ben Amotz, D.; Willis, K. G. *J. Phys. Chem.* **1993**, *97*, 7736.

(28) Bondi, A. *J. Phys. Chem. 68*, **1964**, 441.

(29) Buckingham, A. D. *Proc. R. Soc. London, Ser. A* **1958**, *248*, 169; **1960**, *255*, 32. *Trans. Faraday Soc.* **1960**, *56*, 753.

(30) de Souza, L. E. S.; Guerin, C. B. E.; Ben-Amotz, D.; Szleifer, I. *J. Chem. Phys.* **1993**, *99*, 9954.

(31) Durocher, G.; Sandorfy, C. *J. Mol. Spec.* **1967**, *22*, 347.

(32) Graybeal, J. D. *Molecular Spectroscopy*; 1st ed.; McGraw-Hill: New York, 1976; Chapter 16.

(33) Hershbach, D. R.; Laurie, V. W. *J. Chem. Phys. 35*, **1961**, 458.

(34) Devendorf, G. S.; Ben-Amotz, D.; de Souza, L. E. S. *J. Chem. Phys.* **1996**, *104*, 9858.

(35) Hutson, J. *J. Phys. Chem.* **1992**, *96*, 4237.

(36) Devendorf, G. S., to be published.

(37) Garrabos, Y.; Echargui, M. A.; Marsault-Herail, F. *J. Chem. Phys.* **1989**, *91*, 5869.

(38) Garrabos, Y.; Chandrasekharan, V.; Echargui, M. A.; Marsault-Herail, F. *Chem. Phys. Lett.* **1989**, *160*, 250.

(39) Thibault, F.; Boissoles, J.; Le Doucen, R.; Bouanich, J. P.; Arcas, P.; Boulet, C. *J. Chem. Phys.* **1992**, *96*, 4945.

(40) Morrison, M. A.; Hay, P. J. *J. Chem. Phys.* **1979**, *70*, 4034.

(41) Sverdlov L. M.; Kovner, M. A.; Krainov, E. P. *Vibrational Spectra of Polyatomic Molecules*; John Wiley and Sons: New York, 1974; p 76.

(42) Stull, V. R.; Wyatt, P. J.; Plass G. N. *J. Chem. Phys.* **1962**, *37*, 1442.